Attosecond pulse characterization

G. Laurent*, W. Cao, I. Ben-Itzhak, and C. L. Cocke

James R. Macdonald Laboratory, Physics Department, Kansas State University, Manhattan, Kansas 66506, USA

*glaurent@phys.ksu.edu

Abstract: In this work we propose a novel procedure for the characterization of attosecond pulses. The method relies on the conversion of the attosecond pulse into electron wave-packets through photoionization of atoms in the presence of a weak IR field. It allows for the unique determination of the spectral phase making up the pulses by accurately taking into account the atomic physics of the photoionization process. The phases are evaluated by optimizing the fit of a perturbation theory calculation to the experimental result. The method has been called iPROOF (improved Phase Retrieval by Omega Oscillation Filtering) as it bears a similarity to the PROOF technique [Chini *et al.* Opt. Express **18**, 13006 (2010)]. The procedure has been demonstrated for the characterization of an attosecond pulse train composed of odd and even harmonics. We observe a large phase shift between consecutive odd and even harmonics. The resulting attosecond pulse train has a complex structure not resembling a single attosecond pulse once per IR period, which is the case for zero phase. Finally, the retrieval procedure can be applied to the characterization of single attosecond pulses as well.

OCIS codes: (320.7100) Ultrafast measurements; (140.7240) UV, EUV, and X-ray lasers.

References and links

1. M. Hentschel, R. Kienberger, Ch. Spielmann, G. A. Reider, N. Milosevic, T. Brabec, P. Corkum, U. Heinzmann, M. Drescher, and F. Krausz, "Attosecond metrology," Nature **414**, 509–513 (2001).
2. P. M. Paul, E. S. Toma, P. Breger, G. Mullot, F. Augé, Ph. Balcou, H. G. Muller, and P. Agostini, "Observation of a train of attosecond pulses from high harmonic generation," Science **292**, 1689–1692 (2001).
3. M. Drescher, M. Hentschel, R. Kienberger, M. Uiberacker, V. Yakovlev, A. Scrinzi, Th. Westerwalbesloh, U. Kleineberg, U. Heinzmann, and F. Krausz, "Time-resolved atomic inner-shell spectroscopy," Nature **419**, 803–807 (2002).
4. M. Uiberacker, T. Uphues, M. Schultze, A.J. Verhoef, V. Yakovlev, M.F. Kling, J. Rauschenberger, N.M. Kabachnik, H. Schröder, M. Lezius, K.L. Kompa, H.-G. Muller, M. J.J. Vrakking, S. Hendel, U. Kleineberg, U. Heinzmann, M. Drescher, and F. Krausz, "Attosecond real-time observation of electron tunnelling in atoms," Nature **446**, 627–632 (2007).
5. P. Eckle, A. N. Pfeiffer, C. Cirelli, A. Staudte, R. Dörner, H. G. Muller, M. Büttiker, and U. Keller, "Attosecond ionization and tunneling delay time measurements in helium," Science **322**, 1525–1529 (2008).
6. M. Schultze, M. Fieß, N. Karpowicz, J. Gagnon, M. Korbman, M. Hofstetter, S. Neppl, A. L. Cavalieri, Y. Komninos, Th. Mercouris, C. A. Nicolaides, R. Pazourek, S. Nagele, J. Feist, J. Burgdörfer, A. M. Azzeer, R. Ernstorfer, R. Kienberger, U. Kleineberg, E. Goulielmakis, F. Krausz, and V. S. Yakovlev, "Delay in photoemission," Science **328**, 1658–1662 (2010).
7. K. Klünder, J. M. Dahlström, M. Gisselbrecht, T. Fordell, M. Swoboda, D. Guénot, P. Johnsson, J. Caillat, J. Mauritsson, A. Maquet, R. Taïeb, and A. L'Huillier, "Probing single-photon ionization on the attosecond time scale," Phys. Rev. Lett. **106**, 143002 (2011).
8. A. N. Pfeiffer, C. Cirelli, M. Smolarski, R. Dörner, and U. Keller, "Timing the release in sequential double ionization," Nat. Phys. **7**, 428–433 (2011).

#189466 - $15.00 USD Received 25 Apr 2013; revised 11 Jun 2013; accepted 18 Jun 2013; published 9 Jul 2013

9. A. L. Cavalieri, N. Müller, Th. Uphues, V. S. Yakovlev, A. Baltuška, B. Horvath, B. Schmidt, L. Blümel, R. Holzwarth, S. Hendel, M. Drescher, U. Kleineberg, P.M. Echenique, R. Kienberger, F. Krausz, and U. Heinzmann, "Attosecond spectroscopy in condensed matter," Nature **449**, 1029–1032 (2007).
10. J. Itatani, F. Quéré, G. L. Yudin, M. Yu. Ivanov, F. Krausz, and P. B. Corkum, "Attosecond streak camera," Phys. Rev. Lett. **88**, 173903 (2002).
11. M. Kitzler, N. Milosevic, A. Scrinzi, F. Krausz, and Thomas Brabec, "Quantum theory of attosecond xuv pulse measurement by laser dressed photoionization," Phys. Rev. Lett. **88**, 173904 (2002).
12. Y. Mairesse, A. de Bohan, L. J. Frasinski, H. Merdji, L. C. Dinu, P. Monchicourt, P. Breger, M. Kovačev, R. Taïeb, B. Carréand H. G. Muller, P. Agostini, and P. Salières, "Attosecond synchronization of high-harmonic soft X-rays," Science **302**, 1540–1543 (2003).
13. R. Kienberger, E. Goulielmakis, M. Uiberacker, A. Baltuska, V. Yakovlev, F. Bammer, A. Scrinzi, Th. Westerwalbesloh, U. Kleineberg, U. Heinzmann, M. Drescher, and F. Krausz, "Atomic transient recorder," Nature **427**, 817–821 (2004).
14. E. Cormier, I. A. Walmsley, E. M. Kosik, A. S. Wyatt, L. Corner, and L. F. DiMauro, "Self-referencing, spectrally, or spatially encoded spectral interferometry for the complete characterization of attosecond electromagnetic pulses," Phys. Rev. Lett. **94**, 033905 (2005).
15. Y. Mairesse and F. Quéré, "Frequency-resolved optical gating for complete reconstruction of attosecond bursts," Phys. Rev. A **71**, 011401(R) (2005).
16. F. Quéré, Y. Mairesse, and J. Itatani, "Temporal characterization of attosecond XUV fields," J. Mod. Opt. **52**, 339–360 (2005).
17. Y. Ge., "Quantum enhancement in laser-assisted photoionization and a method for the measurement of an attosecond XUV pulse," Phys. Rev. A **77**, 033851 (2008).
18. J. Gagnon, E. Goulielmakis, and V.S. Yakovlev, "The accurate frog characterization of attosecond pulses from streaking measurements," Appl. Phys. B **92**, 25–32 (2008).
19. H. Wang, M. Chini, S. D. Khan, S. Chen, S. Gilbertson, X. Feng, H. Mashiko, and Z. Chang, "Practical issues of retrieving isolated attosecond pulses," J. Phys. B: At. Mol. Opt. Phys. **42**, 134007 (2009).
20. M. Chini, S. Gilbertson, S. D. Khan, and Z. Chang, "Characterizing ultrabroadband attosecond lasers," Opt. Express **18**, 13006–13016 (2010).
21. J. Gagnon and V.S. Yakovlev, "The direct evaluation of attosecond chirp from a streaking measurement," Appl. Phys. B **103**, 303–309 (2011).
22. W. Cao, G. Laurent, C. Jin, H. Li, Z. Wang, C. D. Lin, I. Ben-Itzhak, and C. L. Cocke, "Spectral splitting and quantum path study of high-harmonic generation from a semi-infinite gas cell," J. Phys. B: At. Mol. Opt. Phys. **45**, 074013 (2012).
23. G. Laurent, W. Cao, H. Li, Z. Wang, I. Ben-Itzhak, and C. L. Cocke, "Attosecond control of orbital parity mix interferences and therelative phase of even and odd harmonics in an attosecond pulse train," Phys. Rev. Lett. **109**, 083001 (2012).
24. G. Laurent, W. Cao, I. Ben-Itzhak, and C. L. Cocke, "Study of Asymmetric Electron Emission in Two-Color Ionization of Helium (XUV-IR)," in *Multiphoton Processes and Attosecond Physics*, K. Yamanouchi and K. Midorikawa, eds., Vol. 125 of Springer Proceedings in Physics (Springer-Verlag Berlin Heidelberg 2012), pp. 173–177.
25. A. F. Starace, "Theory of Atomic Photoionization," in *Handbuch der Physik, Vol. 31*, W. Mehlhorn, ed. (Springer Verlag, Berlin, 1980), pp. 1–121.
26. A.-T. Le, R. R. Lucchese, S. Tonzani, T. Morishita, and C. D. Lin, "Quantitative rescattering theory for high-order harmonic generation from molecules," Phys. Rev. A **80**, 013401 (2009).
27. E. S. Toma and H. G. Muller, "Calculation of matrix elements for mixed extreme-ultravioletinfrared two-photon above-threshold ionization of argon," J. Phys. B: At. Mol. Opt. Phys. **35**, 3435–3442 (2002).
28. J. M. Dahlström, A. L'Huillier, and A. Maquet, "Introduction to attosecond delays in photoionization," J. Phys. B: At. Mol. Opt. Phys. **45**, 183001 (2012).
29. J. M. Dahlström, D. Guenot, K. Klünder, M. Gisselbrecht, J. Mauritsson, A. L'Huillier, A. Maquet, and R. Taïeb, "Theory of attosecond delays in laser-assisted photoionization," Chem. Phys. **414**, 53–64 (2013).
30. J. Mauritsson, P. Johnsson, E. Gustafsson, A. L'Huillier, K. J. Schafer, and M. B. Gaarde, "Attosecond pulse trains generated using two color laser fields," Phys. Rev. Lett. **97**, 013001 (2006).
31. A. T. J. B. Eppink and D. H. Parker, "Velocity map imaging of ions and electrons using electrostatic lenses: Application in photoelectron and photofragment ion imaging of molecular oxygen," Rev. Sci. Instrum. **68**, 3477–3484 (1997).
32. T. Zuo, A. D. Bandrauk, M. Ivanov, and P. B. Corkum, "Control of high-order harmonic generation in strong laser fields," Phys. Rev. A **51**, 3991–3998 (1995).
33. M. Ivanov, P. B. Corkum, T. Zuo, and A. D. Bandrauk, "Routes to control of intense-field atomic polarizability," Phys. Rev. Lett. **74**, 2933–2936 (1995).
34. J. M. Dahlström, A. L'Huillier, and J. Mauritsson, "Quantum mechanical approach to probing the birth of attosecond pulses using a two-colour field," J. Phys. B: At. Mol. Opt. Phys. **44**, 095602 (2011).

#189466 - $15.00 USD Received 25 Apr 2013; revised 11 Jun 2013; accepted 18 Jun 2013; published 9 Jul 2013

1. Introduction

The recent development of x- or extreme-ultraviolet (XUV-EUV) light pulses on an attosecond timescale has opened up new avenues for experimentalists to probe temporal aspects of electron dynamics in atoms, molecules and condensed matter [1, 2]. Both Single Attosecond Pulses (SAPs) and Attosecond Pulse Trains (APTs) have already shown to be very promising tools for the temporal characterization of various atomic processes, such as the delay times in Auger decay [3], tunneling [4, 5], and photoionization [6–9]. In spite of these successful experiments, real-time observation of the electron dynamics is, nevertheless, still in its infancy. This is mainly because the usefulness of such attosecond pulses is limited by the degree to which they can be synthesized in the laboratory. In particular, a precise characterization of such pulses in the time domain still remains a challenging task [10–22].

Because the amplitude of the frequency components making up the pulse can be easily measured with conventional spectrometers, the main challenge for the characterization lies in determining the spectral phase of these components which determine the ultimate length and shape of the pulse in the time domain. To date, the conventional methods dedicated to the phase measurement (namely the RABBITT [2], Streaking [10] and PROOF [20] techniques) rely on the conversion of the attosecond pulse into an electron wave-packet through photoionization of atoms in the presence of a phase-locked IR field. The dressing effect of the IR field on the electron emission oscillates as the time delay between the attosecond and IR pulses is varied. From the characteristics of this temporal modulation, the spectral phases encoded in the electron emission can then be retrieved. The retrieval procedures are generally based on matching measured and simulated temporal modulations. The phases are used as parameters to optimize the fit of the theoretical model to the experimental result. In order to find an iterative solution for these phases in a reasonable amount of time, the simulated temporal modulation is generated from an approximate analytical model of the conversion process, rather than from the "exact" calculation based on numerical solution of the time-dependent Schrödinger equation (TDSE). Even if TDSE calculations would allow an "exact" measurement of the phases, they are still too time-consuming to be efficiently used in an iterative process. As a consequence, the precision of the phase measurement is directly related to the accuracy of the simplified theoretical description of the laser-assisted photoionization process used in the retrieval procedure.

When an APT composed of only odd harmonics is used to ionize an atomic target in the presence of a weak IR field, photoelectrons are observed at energies corresponding to one-photon absorption of the odd harmonics, and, located in between, sideband peaks due to two-photon transitions (absorption of one XUV photon plus absorption or emission of one IR photon). The phases of only two consecutive harmonics are then encoded in the intensity modulation of a given sideband. This allows for a precise and unique determination of the spectral phases of the frequency components making up such kind of APTs *via* the RABBITT technique, based on an accurate description of the two-photon photoionization process within the framework of second-order perturbation theory. The situation changes when the target is ionized with an APT composed of odd and even harmonics or a single attosecond pulse. In these cases, several transitions (at least three) participate to the formation of an electron wave-packet in a given energy state: the direct transition by one XUV photon absorption and several transitions involving absorption of one XUV photon, and absorption (or emission) of one or more IR photons depending on the intensity of the field used in the experiment. The spectral phases of the frequency components involved in all these paths are then encoded in the same electron signal, making the retrieval analysis rather tricky. In order to simplify this analysis, the conventional techniques of characterization of SAPs are based on a simplified description of the conversion of the attosecond pulse into an electron wave-packet in which the contribution of the atomic physics of the photoionization process is not included [20]. However, in a previous study [23],

#189466 - $15.00 USD Received 25 Apr 2013; revised 11 Jun 2013; accepted 18 Jun 2013; published 9 Jul 2013

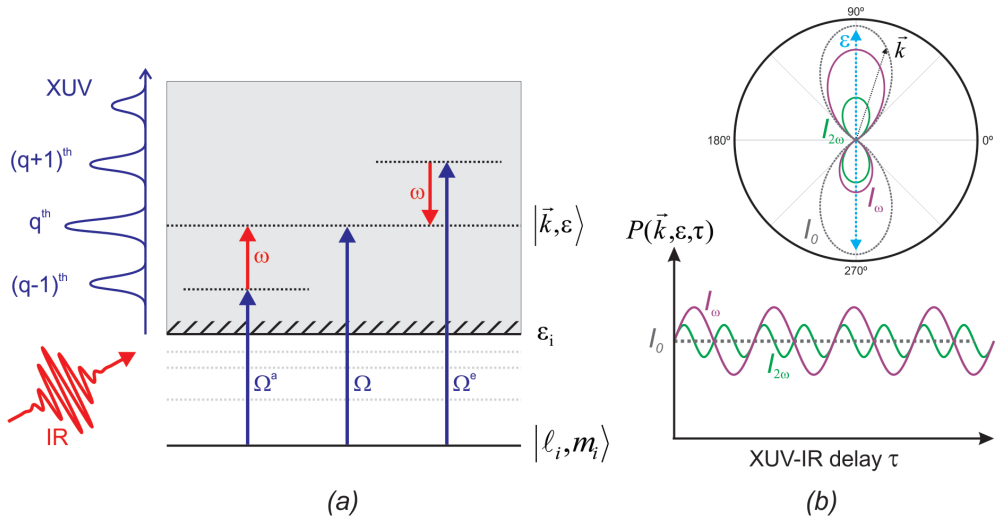

Fig. 1. Principle of the attosecond pulse characterization method. (a) The XUV attosecond pulse is converted into electron wave-packets through photoionization of atoms in the presence of a weak IR field ($\sim 10^{11}$ W/cm^2). Three different quantum paths contribute to the generation of energy-degenerate electron wave-packets in the continuum. Interference between these quantum paths leads to a modulation of the probability of emission $P(\vec{k},\varepsilon,\tau)$ with the time delay τ between the XUV and IR pulses. (b) The probability of emission can be written as the sum of three terms: a constant term I_0 symmetric along the polarization vector direction, an antisymmetric term I_ω oscillating at the IR frequency, and a symmetric term $I_{2\omega}$ oscillating at twice the IR frequency.

we found that such a simplified retrieval procedure, not including the atomic physics, failed to accurately measure the phases of APTs composed of odd and even harmonics. We are thus led to seek a procedure which includes the proper treatment of the atomic physics.

In this work, we demonstrate a new retrieval procedure which allows the determination of the spectral phases of the harmonics making up attosecond pulse train composed of both even and odd harmonics. The procedure explicitly takes into account the atomic physics of the photoionization process. The method is an adaptation of the RABBITT technique for the characterization of attosecond pulse trains composed of only odd harmonics, and bears a strong similarity to the PROOF method for analyzing single attosecond pulses. It relies on the conversion of the attosecond pulse train into electron wave-packets through photoionization of atoms in the presence of a weak IR field ($\sim 10^{11}$ W/cm^2). The description of the photoionization process is based on second order perturbation theory. The fitting algorithm implemented to extract the phase from the modulated electron spectrogram gives unique solutions for these phases.

2. Method

When an IR field of relatively low intensity ($\sim 10^{11}$ W/cm^2) is used to dress the photoionization process, only three different transitions contribute to the generation of energy-degenerate electron wave-packets in the continuum (see Fig. 1(a)): the direct transition induced by absorption of one XUV photon of frequency Ω, and two transitions involving absorption of one XUV photon of frequency Ω^a or Ω^e plus absorption or emission of one IR photon of frequency ω. At a time delay τ between the attosecond and IR pulses, the probability $P(\vec{k},\varepsilon,\tau)$ for emission

#189466 - $15.00 USD Received 25 Apr 2013; revised 11 Jun 2013; accepted 18 Jun 2013; published 9 Jul 2013

of an electron with final momentum $\vec{k}$ and energy ε is then given by the coherent sum of the amplitudes of these three paths, denoted $M_d(\vec{k},\varepsilon)$, $M^a_{cc}(\vec{k},\varepsilon,\tau)$, and $M^e_{cc}(\vec{k},\varepsilon,\tau)$, respectively in Eq. (1):

$$P(\vec{k},\varepsilon,\tau) = |M_d(\vec{k},\varepsilon) + M^a_{cc}(\vec{k},\varepsilon,\tau) + M^e_{cc}(\vec{k},\varepsilon,\tau)|^2, \quad (1)$$

where $\varepsilon = k^2/2 = \Omega - \varepsilon_i$ and $\Omega = \Omega^a + \omega = \Omega^e - \omega$. Interference of the amplitudes for these three quantum paths leads to a modulation of the probability of emission $P(\vec{k},\varepsilon,\tau)$ with the time delay τ. Both the amplitude and the spectral phase of the three frequency components of the attosecond pulse (Ω, Ω^a, and Ω^e) are encoded in this modulation. Provided that the atomic physics of the photoionization process (the conversion process) and the amplitude of these frequency components are known, the temporal analysis of the modulation then provides a way to retrieve the spectral phases.

In our previous study [23, 24], we have shown that the probability of emission $P(\vec{k},\varepsilon,\tau)$ can be written as the sum of three terms (see Fig. 1(b)):

$$P(\vec{k},\varepsilon,\tau) = I_0(\vec{k},\varepsilon) + I_\omega(\vec{k},\varepsilon,\tau) + I_{2\omega}(\vec{k},\varepsilon,\tau). \quad (2)$$

The first term (I_0) is the sum of the probabilities of emission for the one-photon and two-photon processes individually. This term does not depend on the time delay τ, and is symmetric along the polarization vector direction. The second term (I_ω) is an interference term coming from the cross product of the one- and two-photon transition amplitudes, a process that we referred to as First order/Second order Interference (FSI). This interference term represents only a few percent of the total probability of emission when a weak IR field is used in the experiment. It varies sinusoidally with τ at the IR frequency ω, and is antisymmetric along the polarization vector direction. Finally, the last term ($I_{2\omega}$) comes from the cross product of the two-photon transition amplitudes, and describes the interference process the RABBITT technique is based on [2, 12]. This interference term varies sinusoidally with τ at twice the IR frequency, and is symmetric along the polarization vector direction. In general, this term is much weaker than the FSI term as it involves one more photon. The temporal modulation of the probability $P(\vec{k},\varepsilon,\tau)$ with the time delay is then dominated by the FSI term.

It is important to note that the FSI process is not reflected in the total photoionization probability, since the continuum states populated by the one- and two-photon quantum paths are orthogonal to each other. Experimental observation of the FSI modulation thus requires a photoelectron momentum spectroscopy measurement. Even if a complete photoelectron momentum measurement can be readily performed with sophisticated experimental techniques (COLTRIMS, VMI), it is not essential as the measurement of the electron emission along one particular direction is sufficient to observe the FSI modulation. The characterization procedure described in the following is based on the analysis of the temporal modulation of the electron signal detected in one direction along the polarization of the light by making use of state-of-the-art theoretical description of the photoionization process.

3. Theoretical description of the photoionization process.

The low intensity of both the XUV and IR fields allows for a quantum description of the photoionization process within the framework of perturbation theory and the single active electron approximation. The full quantum description of one- and two-photon absorption processes has been described in detail in the literature [25–29]. In this section, we give the general expressions for the one- and two-photon transition amplitudes for an electron emitted in one direction along the polarization vector, and use them to derive the formal expression of the FSI modulation term from Eq. (1).

#189466 - $15.00 USD Received 25 Apr 2013; revised 11 Jun 2013; accepted 18 Jun 2013; published 9 Jul 2013

3.1. One- and two-photon matrix elements

To describe the one- and two-photon ionization process, we have used the results developed by Dahlström *et al.* within the framework of first and second-order perturbation theory and the single active electron approximation [29]. The matrix element for one-photon ionization of the atomic target from its initial states (n_i, ℓ_i, m_i) to the final state (k, ε), with the photoelectron emitted in the positive z direction along the polarization axis $(\hat{z})$ is (see Eq. (47) of Ref. [29]):

$$M_d(k\hat{z}, \varepsilon) = \frac{(8\pi)^{3/2}}{i\sqrt{3}} \tilde{E}_\Omega \sum_\lambda \sqrt{2\lambda+1} \langle Y_{\lambda,m_i} | Y_{1,0} | Y_{\ell_i,m_i} \rangle \langle R_{k,\lambda} | r | R_{n_i,\ell_i} \rangle e^{i\eta_\lambda(k)} \delta_{m_i,0}, \tag{3}$$

where the $Y_{\ell,m}$ are spherical harmonics, the $R_{k,\ell}$ are real radial wavefunctions normalized on the energy scale, $\eta_\lambda(k)$ are the phase-shifts, and $\tilde{E}_\Omega = E_\Omega e^{i\Phi_\Omega}$ is the complex amplitude of the XUV field, with its frequency Ω satisfying $\Omega = \varepsilon + \varepsilon_i = k^2/2 + \varepsilon_i$. The span of accessible angular momentum λ in the final state is governed by the dipole selection rules: $\lambda = \ell_i \pm 1$. The phase-shifts η_λ can be written under the form: $\eta_\lambda(k) = \sigma_\lambda(k) + \delta_\lambda(k) - \lambda\pi/2$, where $\sigma_\lambda(k) = \arg[\Gamma(\lambda + 1 - iZ/k)]$ is the Coulomb phase-shift induced by the ionic core with charge Z, and where the correction $\delta_\lambda(k)$ originates from the short range deviation of the ionic potential from a pure Coulomb potential. Note that only initial states with zero magnetic quantum number, $m_i = 0$, will contribute to photoelectron emission along $\hat{z}$ which is a consequence of the properties of the spherical harmonics along $\hat{z}$: $Y_{\ell,m}(\hat{z}) = \sqrt{(2\ell+1)/4\pi}\delta_{m,0}$.

Similarly, the matrix element for two-photon ionization of the atomic target from its initial states (n_i, ℓ_i, m_i) to the final state (k, ε) *via* the intermediate state $(\kappa, \varepsilon_\kappa)$ with angular momentum λ is (see Eq. (48) of Ref. [29]):

$$M_{cc}(k\hat{z}, \varepsilon, \tau) \approx -\frac{(8\pi)^2}{3\sqrt{2}} \tilde{E}_\omega \tilde{E}_\Omega T(k,\kappa) \sum_L \sqrt{2L+1} \sum_\lambda \langle Y_{L,m_i} | Y_{1,0} | Y_{\lambda,m_i} \rangle \langle Y_{\lambda,m_i} | Y_{1,0} | Y_{\ell_i,m_i} \rangle \times \langle R_{\kappa,\lambda} | r | R_{n_i,\ell_i} \rangle e^{i\eta_\lambda(\kappa)} \delta_{m_i,0}, \tag{4}$$

where

$$T(k,\kappa) = -\frac{1}{\sqrt{k\kappa}} \frac{(2\kappa)^{\frac{iZ}{\kappa}}}{(2k)^{\frac{iZ}{k}}} \Gamma[2 + iZ(\frac{1}{\kappa} - \frac{1}{k})] \Big(\frac{i}{\kappa - k} \Big)^{2 + iZ(\frac{1}{\kappa} - \frac{1}{k})}, \tag{5}$$

and $\tilde{E}_\omega = E_\omega e^{i\omega\tau}$ is the complex amplitude of the IR field. The span of accessible final angular momentum L is governed by the dipole selection rules: $L = \lambda \pm 1 = \ell_i, \ell_i \pm 2$. We note that this two-photon matrix element contains only the phase-shifts η_λ that are governed by the angular momentum λ of the intermediate state, *i.e.* a state that can be reached *via* single-photon absorption.

When applied to the case of noble gases, which are generally first choice targets for the experiment, the non-trivial Eqs. (3) and (4) greatly simplify. In the case of the single ionization of helium atoms ($\ell_i = 0$), these reduce to:

$$\begin{aligned} M_d(k\hat{z}, \varepsilon) &= -i \frac{(8\pi)^{3/2}}{\sqrt{4\pi}} \tilde{E}_\Omega \langle R_{k,1} | r | R_{1,0} \rangle e^{i\eta_1(k)} \\ M_{cc}(k\hat{z}, \varepsilon, \tau) &= -i\tilde{E}_\omega T(k,\kappa) M_d(\kappa\hat{z}, \varepsilon_\kappa). \end{aligned} \tag{6}$$

Similar expressions can be derived in the case of single ionization of neon and argon ($\ell_i = 1$):

$$\begin{aligned} M_d(k\hat{z}, \varepsilon) &= -i4\pi \sqrt{\frac{8}{3}} \tilde{E}_\Omega \Big[\langle R_{k,0} | r | R_{1,1} \rangle e^{i\eta_0(k)} + 2\langle R_{k,2} | r | R_{1,1} \rangle e^{i\eta_2(k)} \Big] \\ M_{cc}(k\hat{z}, \varepsilon, \tau) &= -i\tilde{E}_\omega T(k,\kappa) M_d(\kappa\hat{z}, \varepsilon_\kappa). \end{aligned} \tag{7}$$

#189466 - $15.00 USD Received 25 Apr 2013; revised 11 Jun 2013; accepted 18 Jun 2013; published 9 Jul 2013

3.2. FSI modulation and spectral phases

The FSI modulation I_ω of the electron emission detected along the polarization of the light can be obtained from Eq. (1) by evaluating the cross product of the one- and two-photon transition amplitudes. That is,

$$I_\omega(k\hat{z},\varepsilon,\tau) = 2|M_d|\Big(|M^a_{cc}|\cos\big(\arg[M^*_d M^a_{cc}]\big) + |M^e_{cc}|\cos\big(\arg[M^*_d M^e_{cc}]\big)\Big). \tag{8}$$

Using the simple analytical form of the matrix elements given in Eqs. (6) or (7), and making in Eq. (8) the substitutions $|M^a_{cc}| = E_\omega|T^a||M^a_d|$ and $|M^e_{cc}| = E_\omega|T^e||M^e_d|$, the FSI modulation can be rewritten as:

$$I_\omega(k\hat{z},\varepsilon,\tau) = 2E_\omega|M_d|\Big(|T^a||M^a_d|\cos(\omega\tau+\Delta\Phi^a_\Omega+\varphi^a_{at.}) + |T^e||M^e_d|\cos(\omega\tau+\Delta\Phi^e_\Omega-\varphi^e_{at.})\Big) \tag{9}$$

where M^a_d and M^e_d are the matrix elements associated with the one-photon transition from the ground state to the intermediate states with momentum κ_a and κ_e, respectively, and T^a and T^e are the continuum-continuum matrix elements from those intermediate states to the final state with momentum k. The cosine terms appearing in Eq. (9) describe the interference between each of the two-photon ionization paths ($\Omega^a+\omega$, $\Omega^e-\omega$) and the one-photon transition (Ω). Each of these terms oscillates at the frequency ω of the IR field, and carries a phase $\Delta\Phi^a_\Omega = \Phi_{\Omega^a} - \Phi_\Omega$ ($\Delta\Phi^e_\Omega = \Phi_\Omega - \Phi_{\Omega^e}$) which is the relative spectral phase between the contributing frequency components of the attosecond pulse, and an atomic phase $\varphi^a_{at.}$ ($\varphi^e_{at.}$) equals to the difference in the characteristic phases of the one- and two-photon ionization pathways. These atomic phases are given by:

$$\begin{aligned}\varphi^a_{at.}(k,\kappa_a) &= -\frac{\pi}{2} + \phi_{cc}(k,\kappa_a) + \eta(\kappa_a) - \eta(k)\\ \varphi^e_{at.}(k,\kappa_e) &= -\frac{\pi}{2} + \phi_{cc}(k,\kappa_e) + \eta(\kappa_e) - \eta(k),\end{aligned} \tag{10}$$

where η is the scattering phase-shift of the one-photon matrix element M_d, and ϕ_{cc} is the phase of the continuum-continuum matrix element T.

The two cosine terms appearing in the relation (9) cannot be measured independently. Instead, the measurement of the FSI modulation gives access to the sum of both. For a more direct comparison with the measurement, relation (9) needs to be rewritten in the form:

$$I_\omega(k\hat{z},\varepsilon,\tau) = A_\varepsilon\cos(\omega\tau+\Psi_\varepsilon), \tag{11}$$

where the amplitude A_ε and the phase Ψ_ε are given by:

$$\begin{aligned}A_\varepsilon = 2E_\omega|M_d|\Big(&|T^a|^2|M^a_d|^2 + |T^e|^2|M^e_d|^2\\ &+ 2|T^a||T^e||M^a_d||M^e_d|\cos(\Delta\Phi^a_\Omega - \Delta\Phi^e_\Omega + \varphi^a_{at.} + \varphi^e_{at.})\Big)^{\frac{1}{2}}\end{aligned} \tag{12a}$$

$$\Psi_\varepsilon = \operatorname{atan}\left(\frac{|T^a||M^a_d|\sin(\Delta\Phi^a_\Omega+\varphi^a_{at.}) + |T^e||M^e_d|\sin(\Delta\Phi^e_\Omega-\varphi^e_{at.})}{|T^a||M^a_d|\cos(\Delta\Phi^a_\Omega+\varphi^a_{at.}) + |T^e||M^e_d|\cos(\Delta\Phi^e_\Omega-\varphi^e_{at.})}\right). \tag{12b}$$

The phase retrieval procedure presented in the next section describes the retrieval of the two unknown relative phases $\Delta\Phi^a_\Omega$ and $\Delta\Phi^e_\Omega$, for each harmonic, from the characteristics of the FSI modulation. The relation (12b) shows that a unique solution for these relative phases cannot be determined from the measurement of the phase of the FSI modulation only, as the PROOF technique does. Combining the measurement of both the phase and the amplitude of the modulation, on the other hand, does lead to a unique solution for the relative phases. The relations

#189466 - $15.00 USD Received 25 Apr 2013; revised 11 Jun 2013; accepted 18 Jun 2013; published 9 Jul 2013

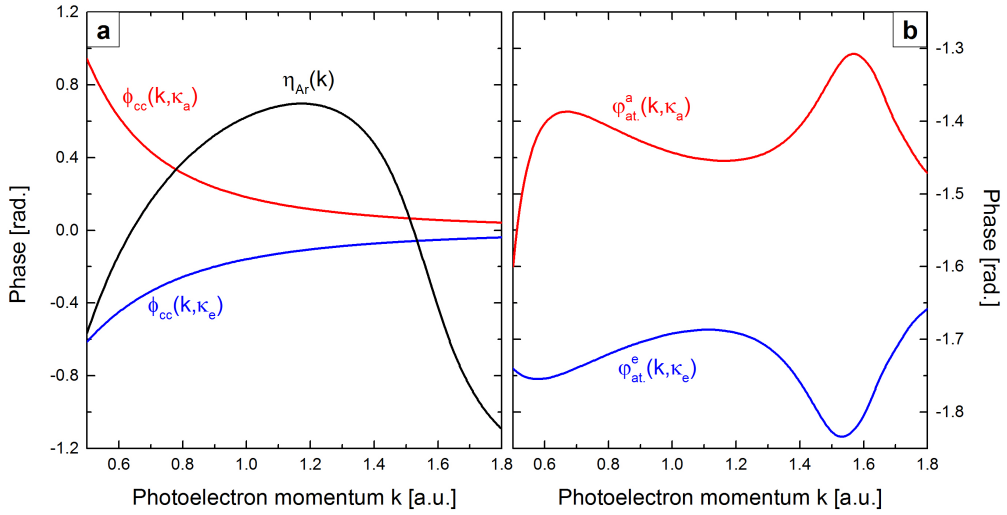

Fig. 2. (a) Scattering phase-shift η of the bound-to-continuum matrix element M_d for argon (black), and continuum-continuum phases ϕ_{cc} for absorption (red) and emission (blue) as a function of photoelectron momentum (taken from Refs. [26] and [29], respectively). (b) Atomic phase difference $\varphi^a_{at.}$ for absorption (red) and $\varphi^e_{at.}$ for emission (blue).

(12) form a system of m coupled equations for the relative phases, where $\Delta\Phi^e_\Omega = \Delta\Phi^a_{\Omega+\omega}$, and $\Delta\Phi^a_\Omega = \Delta\Phi^e_{\Omega-\omega}$, and m is the number of harmonics included in the set. As described below, an iterative solution to such a system results if initial values are assigned to only two variables, one proportional to the value of $\Delta\Phi^a_\Omega$ for the lowest harmonic in the set and the other an overall normalization constant proportional to the IR electric field strength for the whole set. This solution requires that the measured amplitude and phase of the FSI modulation as well as the atomic phases ($\varphi^a_{at.}, \varphi^e_{at.}$) and the matrix elements T and M_d be known for each harmonic. In the procedure described below we use the theoretical values for both the matrix element T (computed with Eq. (5)) and the atomic phases shown in Fig. 2(b). The one-photon matrix element M_d was obtained from the measurement of the photoelectron energy spectrum $S(\varepsilon)$ with only the attosecond pulse present ($S(\varepsilon) \propto |M_d|^2$). Finally, from the retrieved relative phases $\Delta\Phi^a_\Omega$ and $\Delta\Phi^e_\Omega$, the spectral phases Φ_Ω can be deduced by arbitrarily assigning a reference value to one of the harmonics.

4. Phase retrieval procedure

A semi-analytical fitting procedure was used to solve the system of coupled Eqs. (12). The value of $\Delta\Phi^a_\Omega$ for some lower harmonic (for example, the twelfth, when an argon target is used in the experiment) is set equal to some value α. The value of $\Delta\Phi^e_\Omega$ is then found from Eq.(12b), which can be rewritten in the form:

$$\frac{\sin(\Delta\Phi^e_\Omega - \varphi^e_{at.} - \Psi^{exp}_\varepsilon)}{\sin(\Delta\Phi^a_\Omega + \varphi^a_{at.} - \Psi^{exp}_\varepsilon)} = -\frac{|T^a|}{|T^e|}\sqrt{\frac{S(\varepsilon-\omega)}{S(\varepsilon+\omega)}}, \tag{13}$$

where we have used the fact that $S(\varepsilon-\omega) \propto |M^a_d|^2$ and $S(\varepsilon+\omega) \propto |M^e_d|^2$. This equation is solved for $\Delta\Phi^e_\Omega$, and from this result the value of $\Delta\Phi^a_\Omega$ for the next higher harmonic is determined ($\Delta\Phi^a_{\Omega+\omega} = \Delta\Phi^e_\Omega$). In progressing upward through the harmonics, at each photoelectron energy ε, a simple Fourier analysis of the measured electron signal gives both the amplitude $A^{mes.}_\varepsilon$ and

#189466 - $15.00 USD Received 25 Apr 2013; revised 11 Jun 2013; accepted 18 Jun 2013; published 9 Jul 2013

the phase $\Psi_{\varepsilon}^{mes.}$ of the measured FSI modulation.

We note that, for a given value of $\Delta\Phi_{\Omega}^{a}$, Eq. (13) has two solutions:

$$\begin{aligned}
\left(\Delta\Phi_{\Omega}^{e}\right)_1 &= \Psi_{\varepsilon}^{exp} + \varphi_{at.}^{e} + \operatorname{asin}\left[-\frac{|T^a|}{|T^e|}\sqrt{\frac{S(\varepsilon-\omega)}{S(\varepsilon+\omega)}}\sin(\Delta\Phi_{\Omega}^{a} + \varphi_{at.}^{a} - \Psi_{\varepsilon}^{exp})\right] \\
\left(\Delta\Phi_{\Omega}^{e}\right)_2 &= \Psi_{\varepsilon}^{exp} + \varphi_{at.}^{e} + \pi - \operatorname{asin}\left[-\frac{|T^a|}{|T^e|}\sqrt{\frac{S(\varepsilon-\omega)}{S(\varepsilon+\omega)}}\sin(\Delta\Phi_{\Omega}^{a} + \varphi_{at.}^{a} - \Psi_{\varepsilon}^{exp})\right].
\end{aligned} \tag{14}$$

As a consequence, by solving the recurrence equation m times, 2^m possible sets of relative phases are retrieved. The correct solution is the one which minimizes the least squares value:

$$\chi^2(\alpha,\beta) = \sum_m \left[A_{\varepsilon}^{exp} - A_{\varepsilon}^{th}(\alpha,\beta)\right]^2, \tag{15}$$

where A_{ε}^{th} is the simulated amplitude of the FSI modulation at the photoelectron energy ε computed with Eq. (12a), which can be rewritten as:

$$\begin{aligned}
A_{\varepsilon}^{th}(\alpha,\beta) =& \beta\sqrt{S(\varepsilon)}\Big(|T^a|^2 S(\varepsilon-\omega) + |T^e|^2 S(\varepsilon+\omega) \\
&+ 2|T^a||T^e|\sqrt{S(\varepsilon-\omega)S(\varepsilon+\omega)}\cos\left(\Delta\Phi_{\Omega}^{a}(\alpha) - \Delta\Phi_{\Omega}^{e}(\alpha) + \varphi_{at.}^{a} + \varphi_{at.}^{e}\right)\Big)^{\frac{1}{2}},
\end{aligned} \tag{16}$$

and β is an overall normalization factor proportional to the IR electric field strength E_{ω} for the whole set. This procedure is repeated for different values of the boundary condition α and constant factor β, until the $\chi^2(\alpha,\beta)$ minimum is found. The range of possible values for α and β to consider in the fitting procedure can be deduced from Eqs. (12). We can see that adding a constant $k\pi$ ($k \in \mathbb{Z}$) to the phase differences does not change the values of A_{ε} and Ψ_{ε}. This reduces the range of possible value for α to the interval $[0,\pi]$. A close look at the Eq. (12a), on the other hand, shows that the minimum (maximum) possible value for β is achieved when the cosinus term is equal to +1 (-1):

$$\begin{aligned}
\beta^{min}(\varepsilon) &= \frac{A_{\varepsilon}^{exp}}{\sqrt{S(\varepsilon)}\sqrt{|T^a|^2 S(\varepsilon-\omega) + |T^e|^2 S(\varepsilon+\omega) + 2|T^a||T^e|\sqrt{S(\varepsilon-\omega)S(\varepsilon+\omega)}}} \\
\beta^{max}(\varepsilon) &= \frac{A_{\varepsilon}^{exp}}{\sqrt{S(\varepsilon)}\sqrt{|T^a|^2 S(\varepsilon-\omega) + |T^e|^2 S(\varepsilon+\omega) - 2|T^a||T^e|\sqrt{S(\varepsilon-\omega)S(\varepsilon+\omega)}}}
\end{aligned} \tag{17}$$

As the constant factor β has to be the same at all photoelectron energy ε, the range of possible value then reduces to the interval:

$$\beta \in \left[\max\left[\beta^{min}(\varepsilon)\right], \min\left[\beta^{max}(\varepsilon)\right]\right]. \tag{18}$$

Finally, the absolute spectral phases Φ_{Ω} of the harmonics are deduced from the retrieved relative phases by arbitrarily assigning a reference value to one of them.

5. Spectral phase of an APT composed of odd and even harmonics

The retrieval procedure has been applied to the phase measurement and the temporal characterization of an attosecond pulse train composed of odd and even harmonics.

#189466 - $15.00 USD Received 25 Apr 2013; revised 11 Jun 2013; accepted 18 Jun 2013; published 9 Jul 2013

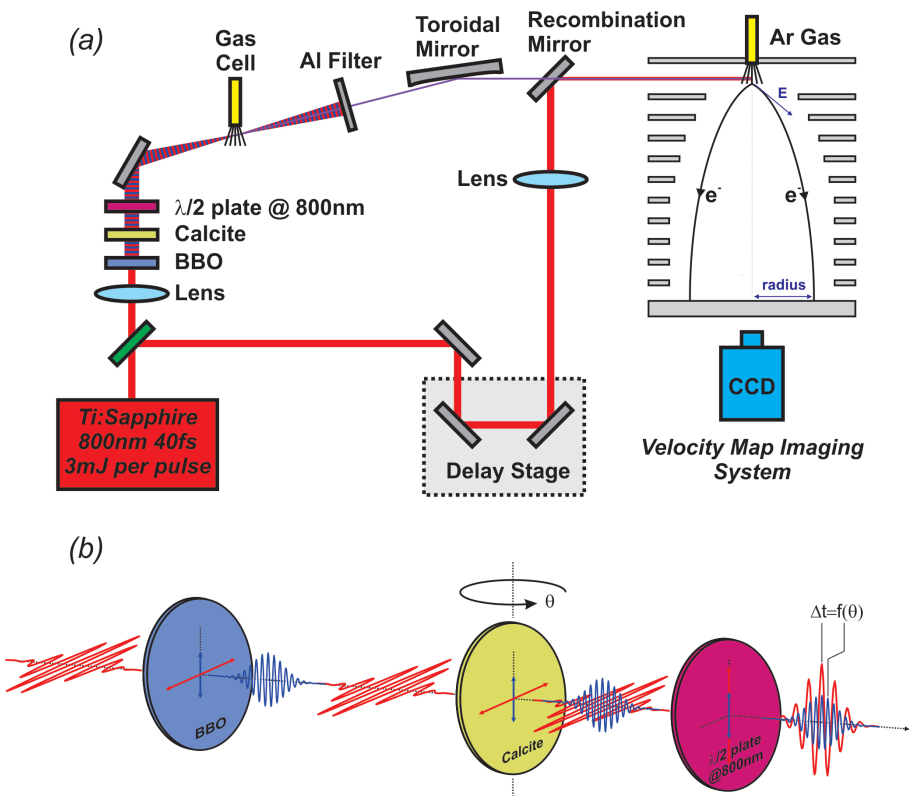

Fig. 3. Schematic view of our experimental setup. (a) The setup combines a Ti:Sapphire laser delivering 40-fs 800-nm pulses at a repetition rate of 1kHz, a XUV-IR Mach-Zehnder interferometer, and a velocity map imaging system. (b) The two-color field used for the high harmonic generation was formed by a collinear optical system composed of a β-barium borate (BBO) crystal, a rotatable calcite plate, and a zero-order half-wave plate at 800 nm.

5.1. Experimental method

The experimental setup used for the measurement combines a Ti:Sapphire laser delivering 40-fs 800-nm pulses at a repetition rate of 1kHz, a XUV-IR Mach-Zehnder interferometer, and a velocity map imaging system (see Fig. 3(a)). Part of the incoming linearly polarized IR beam was sent into the first arm of the interferometer where the APT was generated *via* high harmonic generation with a two-color (800- and 400-nm) field [30]. The field was formed by a collinear optical system composed of a β-barium borate (BBO) crystal, a rotatable calcite plate, and a zero-order half-wave plate at 800 nm (see Fig. 3(b)). The IR beam was first focused by a lens of 50-cm focal length, and then frequency doubled in a 250-μm-thick BBO. A 600 μm birefringent calcite crystal was used to compensate the delay between the resulting orthogonally polarized pulses such that they exactly overlapped in the focal plane. Both pulses were subsequently passed through a zero-order quartz plate which acts as a half-wave plate only for the 800-nm pulse, so that the two pulses exit the quartz plate with parallel polarization. At the exit, the intensity of the 400-nm component was typically 0.5% of that of the 800-nm field. The relative delay between the 800-nm and 400-nm pulses can be adjusted by rotating the calcite crystal about one of its optical axes. The resulting linearly polarized two-color field focused into a 1.5 mm windowless gas cell filled with 10 Torr of argon. The APT was then filtered by

#189466 - $15.00 USD Received 25 Apr 2013; revised 11 Jun 2013; accepted 18 Jun 2013; published 9 Jul 2013

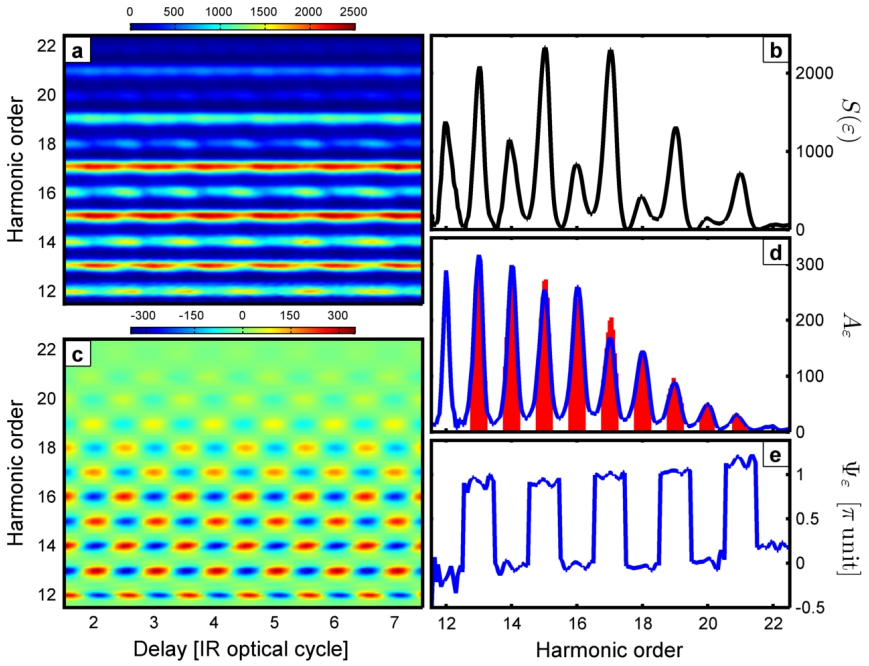

Fig. 4. (a) Photoelectron emission probability from argon measured in one direction along the polarization vector ($\pm$15 deg.) as a function of time delay between the XUV and IR field and the electron energy (in harmonic order unit). (b) Photoelectron spectrum when only the XUV pulse is present. (c) FSI modulation as a function of time delay between the XUV and IR field and the electron energy. (d) Measured (blue line) and simulated (red bars) amplitude of the FSI modulation. (e) Phase of the FSI modulation.

using a spatial aperture (2 mm diameter at 0.5 m) and a 200 nm thick Al thin film to remove harmonics below the 11^{th} order. A replica of the IR (without the 400 nm) was sent into the second arm of the interferometer, whose total length could be changed to vary the time delay τ between the APT and the IR pulse. Both beams were focused, collinearly recombined, and finally sent into a vacuum chamber containing an effusive argon gas jet. At the focal point, the IR intensity is estimated to be below 10^{11} W.cm^{-2}. A velocity map imaging system was used to measure the photoelectrons momenta [31].

5.2. *Data analysis*

The details of the phase retrieval analysis are shown in Fig. 4. The photoelectron emission probability measured along the polarization direction ($\pm$15 deg.) is shown in a density plot as a function of the time delay between the XUV and IR field and the electron energy in Fig. 4(a). At each photoelectron energy ε, a simple Fourier analysis of the electron signal gives the FSI modulation plotted in Fig. 4(c). From the amplitude $A_\varepsilon^{mes.}$ and the phase $\Psi_\varepsilon^{mes.}$ of this modulation, presented in Figs. 4(d) and 4(e), respectively, the relative phase between consecutive harmonics are retrieved. The amplitude of the simulated FSI modulation resulting from the fitting procedure is also shown in Fig. 4(d) (red bars). In order to estimate the accuracy of the analysis, the procedure has been applied successively to retrieve the phase of each frequency component within the harmonic width. The resulting phases have been averaged over the harmonic width, and the standard deviation from the mean value gives an estimated error in the phase measurement of $\pm$5%.

#189466 - $15.00 USD Received 25 Apr 2013; revised 11 Jun 2013; accepted 18 Jun 2013; published 9 Jul 2013

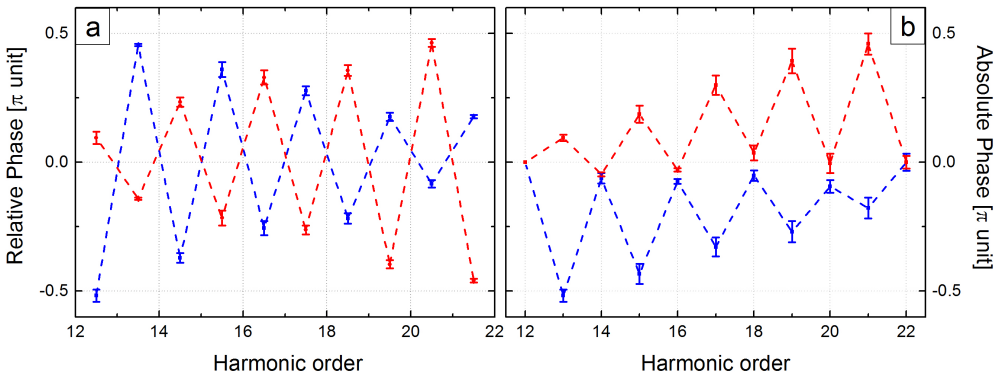

Fig. 5. Relative (a) and absolute (b) spectral phases retrieved by including (blue curve) and neglecting (red curve) the contribution of the atomic physics of the photoionization process in the analysis. The absolute phases have been deduced from the relative phases by arbitrarily assigning zero phase to the harmonic 12.

5.3. Results and discussion

The results of the analysis are shown in Fig. 5. The relative phases between odd and even harmonics are plotted in Fig. 5(a) (blue curve). From these relative phases, the absolute spectral phases of the harmonics are deduced by arbitrarily assigning zero phase to the harmonic 12 (blue curve in Fig. 5(b)). We can observe a large phase shift between consecutive odd and even harmonics in the plateau region. The phase shift is not constant over the entire range of the harmonic orders, though. It decreases (or increases) from $\pi/2$ for the lower harmonics to close to 0 (or π) for the higher ones (our experiment cannot distinguish between these two values). This trend is somewhat different to what we have observed in our previous measurement [23], where we have found a $\pi/2$ even-odd phase shift over the entire plateau region. We note that the procedure used to generate the APT in that previous work, with the polarization of the second-harmonic field orthogonal to that of the IR fundamental, differs from the procedure used here where the polarization of both fields are parallel. This suggests that the quantitative value of the even-odd phase shift may be specific to the procedure used to generate the APT. Further investigation of this question would be a separate, and very worthy, endeavor. We do not yet know of a physical explanation for these phase shifts, but the existence of a phase difference between even and odd harmonics in an APT has been already discussed theoretically. Zuo *et al.* predicted, for harmonics near the cutoff, very large phase shifts, nearly π [32, 33]. Also, a recent calculation of the harmonic generation by a two-color field finds an even-odd phase shift of $\pi/2$ [34], in agreement with the present results for the lower harmonics.

To emphasize the importance of an accurate treatment of the conversion process in the retrieval procedure, we have also carried out a phase retrieval analysis in which the contribution of the atomic physics of the photoionization process is neglected, as is done in the PROOF method. This is achieved by replacing in Eq. (12) the matrix elements M_d, M_d^a, and M_d^e by the strengths of the harmonics E_Ω, E_{Ω_a}, and E_{Ω_e}, respectively, and by setting the matrix elements (T^a,T^e) to one and the atomic phases ($\varphi_{at.}^a$, $\varphi_{at.}^e$) to zero. The relative and absolute phases resulting from this analysis are plotted in Figs 5(a) and 5(b) (red curves). We can observe a significant difference between these phases and the phases retrieved by taking into account the atomic physics of the conversion process. The origin of this discrepancy is mainly, but not uniquely, attributed to the atomic phases of the photoionization process. By not taking into account explicitly the atomic physics in the analysis, the retrieved phases are equal to the relative phases of the har-

#189466 - $15.00 USD Received 25 Apr 2013; revised 11 Jun 2013; accepted 18 Jun 2013; published 9 Jul 2013

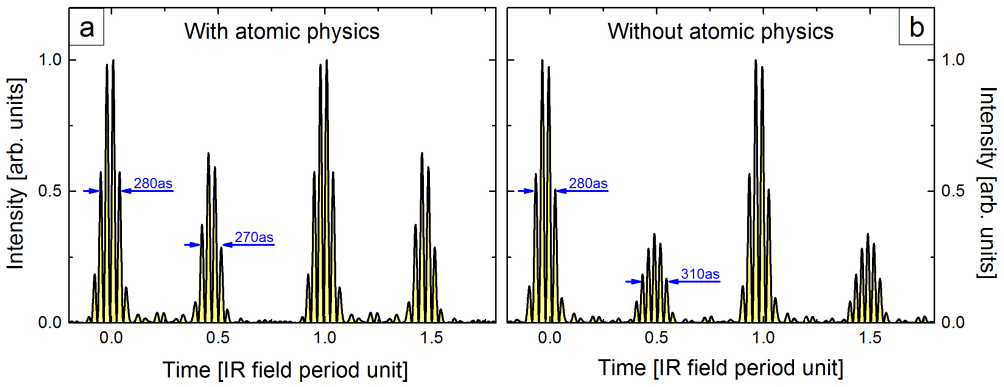

Fig. 6. Temporal profile of the attosecond pulse train retrieved by including (a) and neglecting (b) the contribution of the atomic physics of the photoionization process in the analysis.

monic plus the atomic phases. As shown in Fig. 2(b), these atomic phases are close to $-\pi/2$. This leads to an opposite trend for the phase shifts between consecutive odd and even harmonics as a function of the harmonic order. The phase shift now increases from 0.1π for the lower harmonics in the plateau region to $\pi/2$ for the higher ones. Obviously, this difference in the retrieved phases also leads to a difference in the temporal profile of the reconstructed attosecond pulse train as shown in Fig. 6. These temporal profiles have been reconstructed from the phases shown in Fig. 5(b) and the amplitudes deduced from the photoelectron energy distribution shown in Fig. 4(b) by correcting for the different photoionization cross sections [26]. In both cases, the reconstruction leads to a train formed by a series of two pulses, one more intense than the other. Even though the two analysis methods, with and without including the atomic physics, lead to a similar duration for each of these pulses ($\sim$ 300 as), the temporal envelopes of the reconstructed trains are distinct. We can see that the analysis done without taking into account the atomic physics of the conversion process underestimates the intensity of the second pulse.

Finally, it is interesting to notice the implications the phase-shift between consecutive odd and even harmonics has for the physical picture of the electric field of the APT. It is often assumed, even stated, that the combination of even and odd harmonics in the pulse train creates a series of pulses which occur only once per cycle, rather than half when only odd harmonics are present in the pulse, and thus offer the possibility to "strobe" an atom or molecule only once during each IR cycle. The temporal profile of the APT shown in Fig. 6 contradicts this nice physical picture. The picture holds only if there is no phase shift between even and odd harmonics. If the even-odd phase shift is different from zero, as our measurement suggests it can be, the resulting APT has a more complex structure not resembling a single AP once per IR period. It is still correct that the repetition time of the pulse is a full optical cycle, but the waveform becomes a more complex and extended pulse.

6. Conclusion

In this work, we have demonstrated a novel procedure for the characterization of attosecond pulses, termed iPROOF (improved Phase Retrieval by Omega Oscillation Filtering) for its similarity with the already existing PROOF technique. The method relies on the conversion of the attosecond pulse into electron wave-packets through photoionization of atoms in the presence of a weak IR field. The spectral phases of the frequency components making up the pulse are

#189466 - $15.00 USD Received 25 Apr 2013; revised 11 Jun 2013; accepted 18 Jun 2013; published 9 Jul 2013

determined from the temporal modulation of electron signal detected in one direction along the polarization of the light, as the delay between the attosecond pulse and the IR field is varied. The main advantage of our method over other techniques is that it allows for the unique determination of these spectral phases by accurately taking into account the atomic physics of the photoionization process. The phases are evaluated by optimizing the fit of a state-of-the-art two-photon perturbation theory calculation to the experimental result. Because only two parameters, the phase of a particular frequency component and a normalization factor proportional to the IR electric field strength, are used in the fit, our semi-analytical retrieval procedure is much faster than other techniques based on evolutionary algorithms which use all the phases as parameters for the optimization. The retrieval algorithm is also robust and does not need any initial assumption about the phases. The measurement is easy to setup at low cost as it only needs the measurement of the photoelectron emission in one direction along the polarization vector, which can be easily done with a conventional time-of-flight spectrometer.

Finally, because the procedure allows the measurement of the spectral phases of the frequency components that are coupled by the IR field, it is then suitable for the characterization of attosecond pulse trains with discrete spectra composed of odd and even harmonics. Moreover, it can also be applied to the characterization of single attosecond pulses, even if such pulses cover a continuous spectrum. This can easily be done by successively and independently applying the procedure to each subset of frequency components in the spectrum that are coupled by the IR field.

Acknowledgments

We thank A. T. Le for providing us with the model phase shifts and radial matrix elements for Ar. This work was supported by three funding agencies. The main funding was provided by the Chemical Sciences, Geosciences, and Biosciences Division, Office of Basic Energy Sciences, Office of Science, U.S. Department of Energy. In addition, the U.S. Army Research Office under Grant No. W911NF-071-0475 provided the laser and the interferometer. The National Science Foundation under Grant No. CHE-0822646 provided the imaging setup and supported W. C. partly.

#189466 - $15.00 USD Received 25 Apr 2013; revised 11 Jun 2013; accepted 18 Jun 2013; published 9 Jul 2013